Detection of the key steps during Liquid Resin Infusion manufacturing of a polymer-matrix composite using an in-situ piezoelectric sensor

Corentin Tuloup, W. Harizi, Zoheir Aboura, Yann Meyer, B. Ade, Kamel Khellil

Version of Record: https://www.sciencedirect.com/science/article/pii/S2352492819312711
Manuscript_bce85ee65f28e88535f3542582740b00

Detection of the key steps during Liquid Resin Infusion manufacturing of a polymer-matrix composite using an in-situ piezoelectric sensor.

C. Tuloup[1,*], W. Harizi[1], Z. Aboura[1], Y. Meyer[1,2] , B. Ade[1], K. Khellil[1]

[1]*Alliance Sorbonne Université, Université de Technologie de Compiègne, Laboratoire Roberval de Mécanique FRE UTC-CNRS 2012, Dept IM, CS 60319, 60203 Compiègne Cedex, France*

[2]*Univ. Bourgogne Franche-Comté, UTBM, F-90010 Belfort, France*

[*] Corresponding author: corentin.tuloup@utc.fr

Abstract

This article investigates the interest of a novel promising approach, dealing with the use of an in-situ piezoelectric (PZT) disk to monitor the whole manufacturing process of a glass fiber/polyester Polymer-Matrix Composite (PMC) plate using the Liquid Resin Infusion (LRI) technique. The real-time in-situ Process Monitoring (PM) is conducted using the electrical signature (capacitance) variation of the embedded PZT transducer, which has never been done so far in the literature for such a purpose. In order to understand the capacitance response, an internal/external multi-instrumentation (Infrared Thermography, thermocouples, Acoustic Emission, Z-displacement and pressure sensing devices) was set on the infusion systems, so that it was possible to make multi-physical couplings between the various obtained measurements and the PZT capacitance curves. It was shown that the PZT capacitance is sensitive to all several steps of the infusion process, especially the gelation and vitrification phases, and can also have Structural Health Monitoring (SHM) applications as it makes the resulting composite part “smart”.

Keywords: Polymer-matrix composites (PMCs); In-situ piezoelectric sensor; Process monitoring; Non-destructive testing; Vacuum infusion.

Glossary (by order of appearance within the text)

Abbreviation	Designation
LCM	Liquid Composite Moulding
RTM	Resin Transfer Moulding
LRI	Liquid Resin Infusion
PMC	Polymer-Matrix Composite
PM	Process Monitoring
FRP	Fiber Reinforced Polymer
NDT&E	Non-Destructive Testing and Evaluation
DEA	Dielectric Analysis
DC	Direct Current
ETDR	Electrical Time Domain Reflectometry
OFI	Optical Fiber Interferometry
US	Ultrasound
OFR	Optical Fiber Refractometer
TC	Thermocouple
OF	Optical Fiber
IRT	Infrared Thermography
DSC	Differential Scanning Calorimetry
DMA	Dynamic Mechanical Analysis
SHM	Structural Health Monitoring
LZT (PZT)	Lead Zirconate Titanate
AE	Acoustic Emission
LVDT	Linear Variable Differential Transformer
A-US	Acousto-Ultrasound
IMPS	In-Mould Pressure Sensor
MCR	Modular Compact Rheometer
MEKP	Methyl Ethyl Ketone Peroxide
CAE	Cumulative Absolute Energy
ROI	Region Of Interest

1. Introduction

In composite materials industry, manufacturing parameters of Liquid Composite Molding (LCM) processes (Resin Transfer Molding (RTM), Liquid Resin Infusion (LRI), etc.) such as mold filling rate, permeability, preform impregnation quality or resin curing kinetics are relatively difficult to evaluate. Their knowledge can be very helpful to improve these processes and obtain Polymer-Matrix Composite (PMC) parts with better mechanical properties and tolerances. As this subject is of paramount importance since the appearance of PMC in industry, many scientific teams have already worked on it, and the found literature is very abundant. Various ex and in-situ techniques are used to follow and understand the multiple phenomena occurring during manufacturing, which are commonly attributed to Process Monitoring (PM). Konstantopoulos et al. [1] dedicated a whole literature review to the different measuring means employed to perform PM of Fiber Reinforced Polymer (FRP) composites. These reviews and other references listed many Non-Destructive Testing (NDT) techniques such as Dielectric analysis (DEA: [2–8]), Direct Current (DC:[9–13]) analysis, Electrical time domain reflectometry (ETDR: [14–18]), Optical Fiber Interferometers (OFI: [19–23]), Ultrasonic (US: [24–37]) transducers, Optical fiber refractometers (OFR: [38–43]), spectrometers ([43–48]), thermometers (thermocouples (TC), optical fibers (OF), Infrared Thermography (IRT)) ([2,38,49–54]) or pressure transducers ([55–63]). According to the sensing technique, it is possible to follow manufacturing parameters such as the flow front, the resin viscosity, the curing degree, the events during cure such as gelation, the detection of air bubbles, the void amount or the compaction pressure. However, many other contributions to the PM of PMCs can be found in the literature, such as the use of optical cameras ([64], [54]) or dial gauges [62] to infer in-plane [64] or out-of-plane (fabric thickness evolution: [54], [62]) deformation of reinforcements due to the passing of the resin flow; and combined optical (camera) and pressure measurements to evaluate fabric unsaturation during the preform impregnation [65] or to analyze resin flow/pressure and fabric compaction/thickness evolution ([61], [63]). Electrical measurements were also employed to follow fibers impregnation [66], resin flow [67]; and cure behavior ([68–72]), as well as calibrated test benches [73], electrical measurements [74] or models [75] to evaluate reinforcement permeability. The resin mass flow rate can also be evaluated in real-time thanks to the use of a mass balance supporting the resin container [63]. As process-induced strains are also of great interest for the manufactured part to be used in service, it is also possible to monitor them using OF sensors ([21,76–79]). Employing the manufactured composite as the process monitoring sensor has also been investigated, using (coated or not) piezoresistive fabrics [80–83] to follow parameters such as preform compaction, resin flow, cure, resin state transitions or residual stress. Active control of a manufacturing process, meaning not only passive information gathering, is also feasible; where researchers can follow the preform impregnation and potential resin flow disturbances with a camera and automatically adjust resin flow in real-time with a connected injection ports system [84]. Other ex-situ techniques, such as Differential Scanning Calorimetry (DSC) [85], Dynamic Mechanical Analysis (DMA) [86] or rheology [87] can help to characterize the matrix and understand its behavior during manufacturing, but the major inconvenient is that they are not performed at the same time as the manufacturing process, meaning no real-time measurements, and only on small samples mainly made of pure resin which neglects the fiber impact on the results.

Among all the previously cited PM techniques, some of them are ex-situ and some others in-situ, depending on their way of working and level of cumbersomeness. However, the actual trend in research deals with the use of embedded “smart” structures, with auto-checking abilities. There are indeed several advantages to use in-situ NDT devices to perform a real-time PM: First, the potential cumbersomeness of the ex-situ devices is avoided, as the

embedded system is an integral part of the composite material. As a result, this system can gather information about the state of its host during its whole lifecycle, from the manufacturing stage (PM) to the life in service (Structural Health Monitoring or SHM). Another positive point is the potential increase in sensitivity during the measurement, as the measuring NDT device is incorporated at the heart of the material and not positioned on its surface or remotely. Finally, the in-situ NDT system can be protected from the potentially harsh environments such as temperature, humidity, mechanical loadings, etc. when the manufactured composite part will be used in service. The presented literature deals with a variety of manufacturing techniques, from LCM such as Liquid Resin Infusion (LRI) or Resin Transfer Moulding (RTM) to filament winding and autoclave processing. All these techniques are used at the industrial scale, but one can see a rise in the use of LRI for manufacturing technical parts nowadays, especially in wind and shipbuilding [55]. This is mainly due to the fact that LRI allows to manufacture parts with big dimensions and complex geometries in one shot, with no need for further machining. Other techniques, such as RTM or autoclave, are limited by the size and complexity of the molds (for RTM) and by the size of the pressurized oven and especially the price (for autoclave). Consequently, LRI is considered to be a serious competitor of autoclave and RTM for the future.

Considering the last two developed points, extending research on real-time in-situ PM of LRI manufacturing would be of great interest, with the aim of improving the knowledge about the related process parameters and obtaining “smart” parts with optimal quality able to perform in-situ SHM. This is what the authors propose in this study: an in-situ thin piezoelectric Lead Zirconate Titanate (LZT or PZT) transducer is inserted inside a dry glass fiber stack to perform in-situ and real-time PM of a glass fiber/polyester resin composite plate manufactured by LRI, the whole manufacturing stage being continuously monitored with an external/internal multi-instrumentation involving 4 Acoustic Emission (AE) sensors, 1 pressure sensor, 1 IRT camera, 2 Linear Variable Differential Transformer (LVDT) and 2 TCs. Polyester resin chemo-physical characterization is also performed aside, using oscillatory rheology. The PZT electrical capacitance variations during the whole process are combined to the multi-physical couplings obtained with the multi-instrumentation and the matrix behavior inferred by rheological testing. The authors highlighted the potential of the PZT to be sensitive to several key moments of LRI manufacturing, such as end of preform impregnation, end of resin injection, and especially resin state transitions which are gelation and vitrification. This article stands out of the previous papers investigating the same area ([2,6,8,22,37,39,43,83] and others) by the use of the in-situ PZT in both passive (electrical measurements gathering) and active modes, the last one allowing to follow the resin curing with an Acousto-Ultrasonic (A-US) approach using the waves continuously generated by the PZT when connected to a multimeter for capacitance measurements. Moreover, the use of a multi-instrumentation comprising such a number of various NDT techniques to combine them into multi-physical couplings and associate these ones with the PZT signature and rheological data as well to understand the occurring phenomena as accurately as possible, has never been undertaken until now to the authors’ knowledge. Non-Destructive Testing and Evaluation (NDT&E) techniques are especially used for the Structural Health Monitoring (SHM) of composite structures, to realize real-time surveillance of PMC materials during some mechanical loading [88–90]. However, very few works are using this number of NDT&E techniques for the PM of these structures.

First, the conducted experiments are detailed in the next section. Then, after a short theoretical background about resin chemo-physical characterization, the obtained results will be presented. The authors will first focus on the multi-physical couplings occurring during LRI manufacturing in the first place, and then on the sensitivity of the PZT to the polyester resin

state transitions during curing when confronting the PZT electrical signature to the resin chemo-physical characterization data obtained during a cure cycle. A concluding section discussing the potential of the PZT and its further applications will end this paper.

2. PMC Materials and experimental methods

PZT sensor discs (Wealthland – China, 0.076 USD/each) and with 25mm in diameter and 0.135mm in thickness are used in this study (**Figure 1**. a). Their choice was motivated by several reasons, such as their cheapness, their potential low intrusiveness due to their small dimensions, and finally their possible use in both active (actuator) and passive (sensor) modes. All these reasons made them perfect candidates to create "smart" structures for in-situ and real-time future SHM applications. Their static capacitance was firstly tested with a digital multimeter to confirm the datasheet provided by the manufacturer, before their embedding and wiring in the middle plane of each fiber stack with 1 PZT per stack, as presented in **Figure 1**. b and c. This positioning was chosen to equilibrate/remove the potential residual stresses which could occur during resin consolidation and thus compress the PZT in an inhomogeneous way. The wiring of the PZTs was done using tinned copper wires of 210 µm in diameter. All stacks were then prepared for the LRI operation (**Figure 2**), performed at ambient temperature in an air-conditioned room, with a fixed hardener concentration. All important details about the materials used for this manufacturing can be found in **Table 1**.

(a)

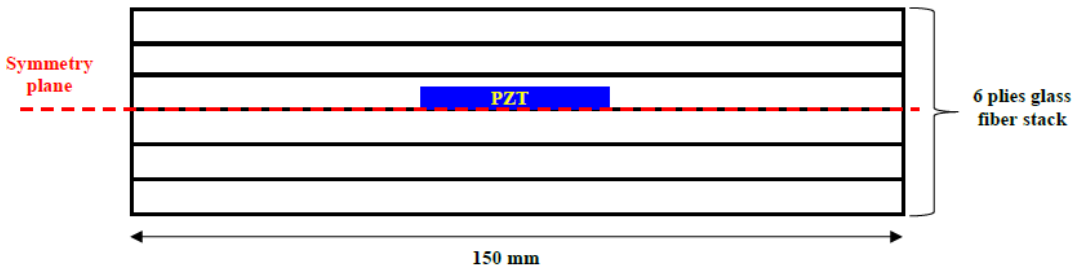

(b)

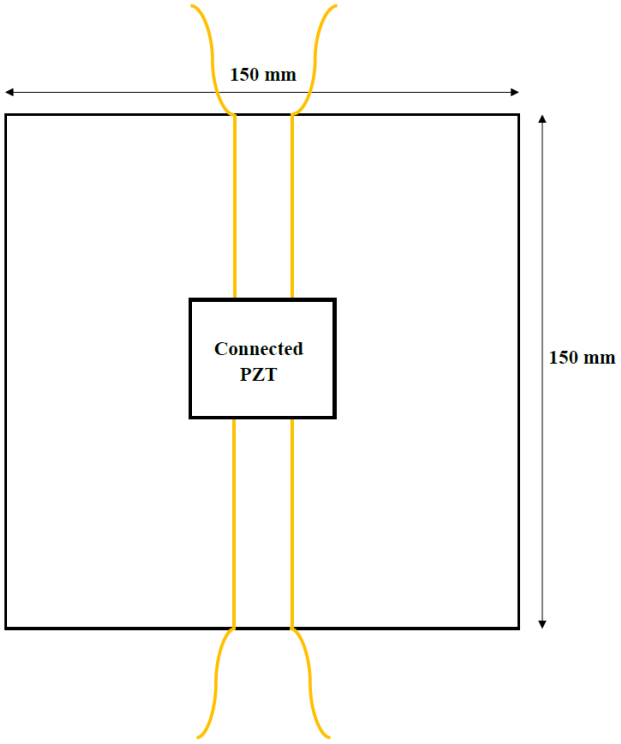

(c)

Figure 1. *(a) PZT sensor disc, (b) Through-the-thickness position of the PZT, (c) Wiring of the PZT on the top of the third ply*

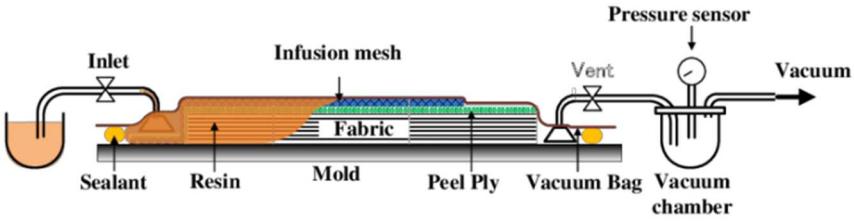

Figure 2. *Scheme of the LRI manufacturing technique* [91]

During manufacturing, a multi-instrumentation test set-up with internal and external devices was realized to gather real-time information about the process. It included an IRT camera, 2 thermocouples, 2 LVDT Z-displacement sensors, 4 AE sensors, 1 pressure sensor and a multimeter for the measurement of the in-situ PZT electrical capacitance. These different devices were positioned on the composite plate as shown in **Figure 3.** All the useful details about this multi-instrumentation can be found in **Table 2**.

Chemo-physical characterization tests of the matrix were also done, using a parallel plate rheometer, whose information are gathered in **Table 3**. The final test set-up is illustrated in **Figure 4**. The data acquisition and demolding of the plates were done 6 hours after resin injection, to be sure of their quasi-complete curing. To plot all these different data together in the same graph, a simultaneous trigger of all used instrumentation was mandatory and based

on the beginning of the previously degassed resin injection. Eight minutes are the necessary time between the resin/hardener mixing and the beginning of the injection operation into the infusion system. This time was also respected for each rheological test, between the mixing and the beginning of the rotation of the superior plate of the rheometer after contact with the mixture. Thereby, it was possible to plot the rheological data with the infusion ones in the same graph.

During the experimental testing, 3 plates were manufactured with a 1wt.% hardener concentration. The manufacturing of a PMC plate embedding a PZT sensor, from the woven glass cutting stage to the demolding phase, requires 4 days of work because it's a thorough task especially with the implementation of the different NDT&E techniques. Concerning the rheological samples with the same hardener concentration, 3 repeatabilities were also made.

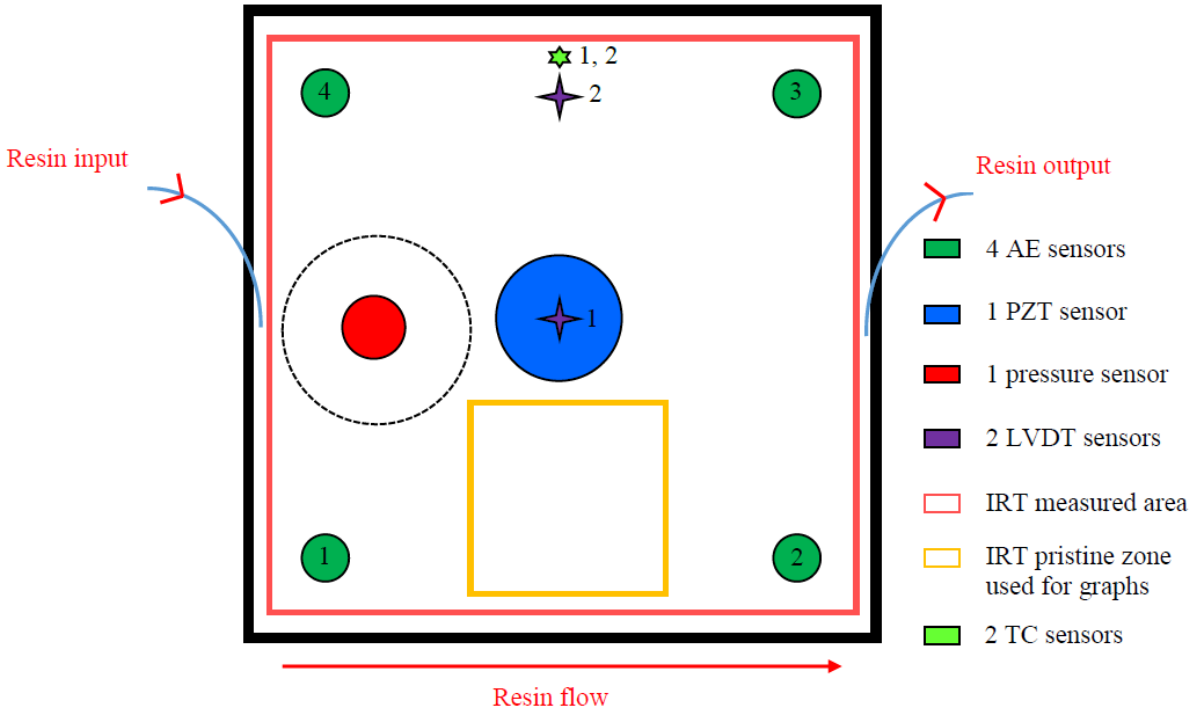

Figure 3. *Sketch of the multi-instrumented LRI system*

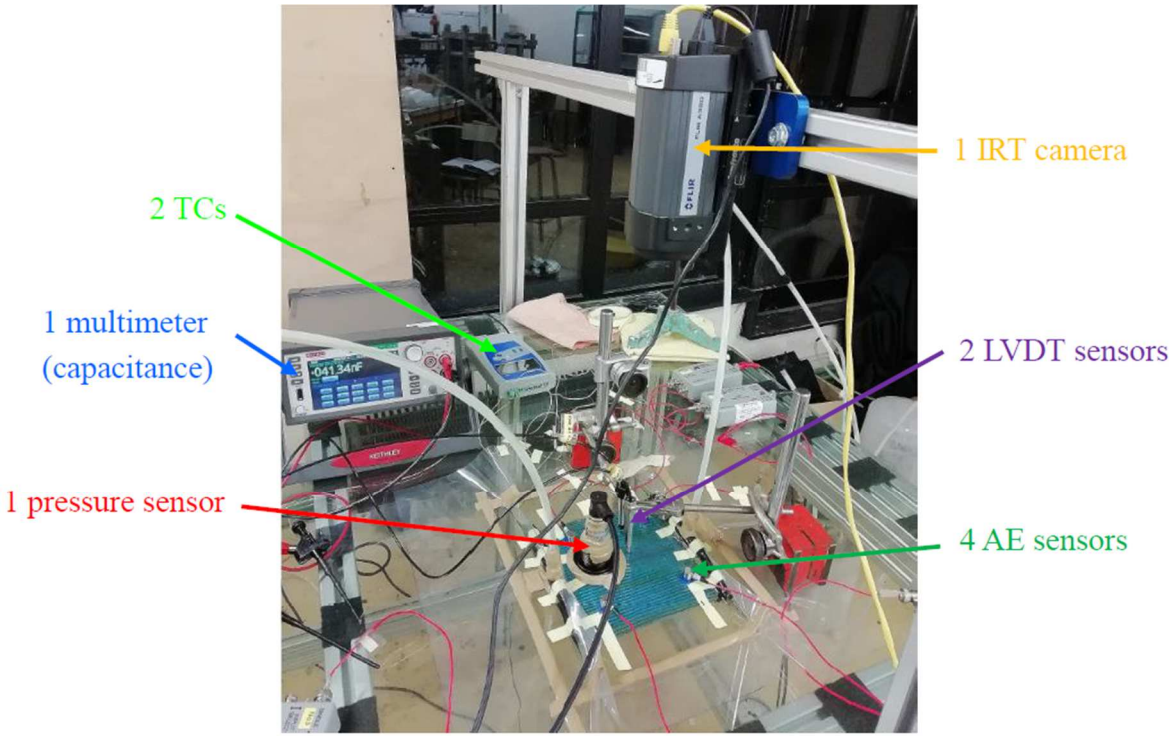

Figure 4. *Experimental devices used for the PM of the LRI process*

Table 1. *Materials and parameters used for LRI manufacturing*

Material	Denomination	Used quantities per plate
Fibers	▪ Glass 2/2 twill fabric with 0.2mm in thickness and a surface mass of 280g/m² (**Gazechim Composites**)	- 6 plies of 150*150mm² - Fiber volume rate = 50%
Matrix	▪ Orthophthalic unsaturated Polyester resin (pre-accelerated) Norester 822 Infusion. (**Nord Composites**)	- 300 g (the excess used to expel as many air bubbles as possible from the infusion system) - Degassing pressure: -0.4Bar (4 minutes) - Injection pressure: -0.65Bar
Hardener	▪ Methyl ethyl ketone peroxide (MEKP) Ketanox B180 (**C.O.I.M s.p.a**)	- 1wt.%

Table 2. *NDT techniques and parameters used for the multi-instrumentation*

NDT technique	Corresponding instrumentation	Experimental parameters
Acoustic Emission (external)	▪ 4 PAC Micro80 sensors (200-900 kHz) glued with Loctite SI5926 Blue Silicone grease (coupling interface). ▪ Acquisition system: AEwin software. (**Physical Acoustics Corporation-Mistras Group)**	- Threshold acquisition: 35dB - Preamplifier gain: 40dB
Infrared Thermography (external)	▪ IR camera FLIR A320. Sensitivity: <50 mK (320*240 pixels) ▪ Acquisition system: FLIR ResearchIR Max software. **(FLIR Systems)**	- Acquisition frequency: 1 Hz - The whole plate is covered by the detector
Thermocouples (internal)	▪ 2 « T »-TC sensors. (**TC S.A. France**) ▪ Acquisition system: DaqPRO 5300. **(Fourier Systems)**	- Position: 1 in the middle of the fiber stack, 1 on the top of the fiber stack, under the vacuum bag - Acquisition frequency: 0.1 Hz
Pressure measurement (external)	▪ 1 In Mould Pressure Sensor (IMPS -1 to 3bar, 0-10 Volts) connected to a display housing. **(Composite Integration)**	- Position: over a small hole drilled inside the vacuum bag.
Z-displacement of the surface of the infused plate (external)	▪ 2 LVDT sensors (1.25mm/Volt - ±2.5mm displacement & 0.5mm/Volt - ±1mm displacement) connected to a Modular 600 setting box. **(RDP Electronics Ltd)**	- Position: vertical, on the vacuum bag. One at the PZT embedding position and one aside on the pristine preform.
Capacitance measurement (internal)	▪ 1 DMM7510 digital multimeter Resolution: 3 to 7 digits (up to 0.1 pF) **(Keithley)**	- Connected to PZT wires exiting the plate. - Acquisition frequency: 2 Hz
Acquisition system	▪ Connected to the two LVDT sensors and to the IMPS pressure sensor. **(Device and software made by UTC electronic department)**	- Acquisition period: 0.7s

Table 3. *Instrumentation and parameters used for chemo-physical characterization*

Characterization method	Corresponding	Experimental parameters

	instrumentation	
Oscillatory rheology	▪ Modular Compact Rheometer (MCR) 502 with disposable plane/plane measuring system. ▪ Acquisition system: Rheoplus software **(Anton Paar)**	- Sample: 3g of resin mixed with the 1wt.% amount of hardener. - Protocol: ambient temperature, rotation frequency = 1Hz, deformation γ = 1%, test conducted until stabilization of the second complex viscosity modulus (as a function of time).

3. Theoretical background

Here is going to be detailed how the authors used oscillatory rheology measurements (dynamic loading) to characterize the resin used for the infusions during its curing stage. The idea is to highlight the different chemo-physical state transitions which can occur during resin curing. As the used polyester matrix is a thermoset, it can undergo several of these transitions according to the literature: gelation, vitrification, cure-induced phase separation or devitrification [92], but the authors will only focus on the first two ones, as the others are not involved during the presented infusion process. Gelation allows the resin to transform from a liquid to a gel form (rubber phase), then the latter toughens itself until it becomes a glass which corresponds to the vitrification stage. After this second main event, the reaction rate slows down even if the temperature is increased, or stops [92]. As the studied resin has an intrinsic viscoelastic behavior, its stress reaction σ when submitted to a periodic oscillatory shear stress $\gamma = \gamma_0 \exp(i\omega t)$ with a small amplitude can be described using **Equation 1**:

$$\sigma = \sigma_0 \exp(i\omega t + \delta) \qquad \textbf{Equation (1)}$$

where ω is the pulsation of the solicitation, and δ the phase between the original strain signal and the obtained material stress response. σ and γ are linked by a complex shear modulus G^* by the following relation: $\sigma(t) = G^*(\omega)\gamma(t)$, with $G^* = G' + iG''$involving *G'* as the storage modulus and *G''* as the loss modulus. The storage modulus *G'* is associated with the elastic behavior of the resin, when energy coming from the outside can be stored and then given back by the system, and the loss modulus *G''* characterizes its viscous behavior when the received energy is dissipated through the moving chains of the polymer instead of being returned. These two variables both appear in the complex viscosity expression η_*, shown in **Equation 2**. The three variables, $|\eta_*|$ (in modulus), *G'* and *G''* will be measured and plotted in real-time when performing the oscillatory rheology tests. First of all, gelation will be highlighted by the crossing of *G'* and *G''* [93–95], this crossing being normally associated with a rise of the viscosity complex modulus $|\eta^*|$ curve as a function of the time. Then, the maximum of *G''* before its final drop will point out vitrification [96], because at this time the resin, as a solid glass, has no remaining viscous properties.

$$\eta_* = \frac{G''}{\omega} - i\frac{G'}{\omega} \qquad \textbf{Equation (2)}$$

4. Results and discussions

4.1.Multi-instrumented infusion: couplings between the different in and ex-situ signatures

The results of the multi-instrumented infusion for a reference manufactured plate are shown in **Figure 5**. Two other plates were manufactured for repeatability, and the corresponding curves are displayed in **Figure 6** & **Figure 7**. An example of the obtained composite plate is illustrated in **Figure 8**.

a. Resin injection stage

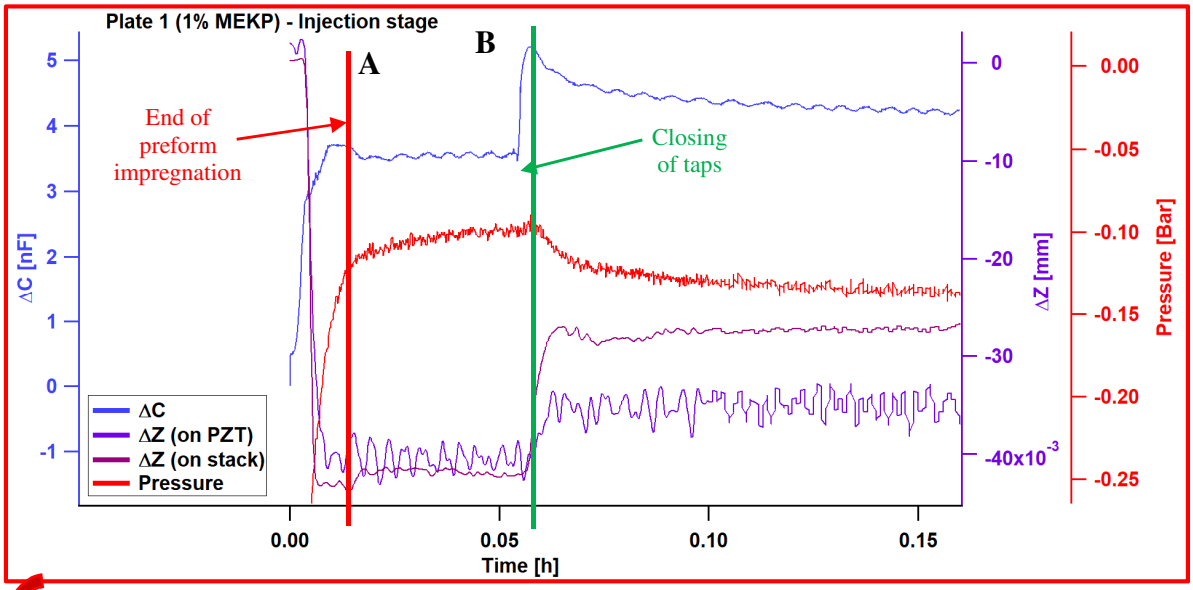

(a)

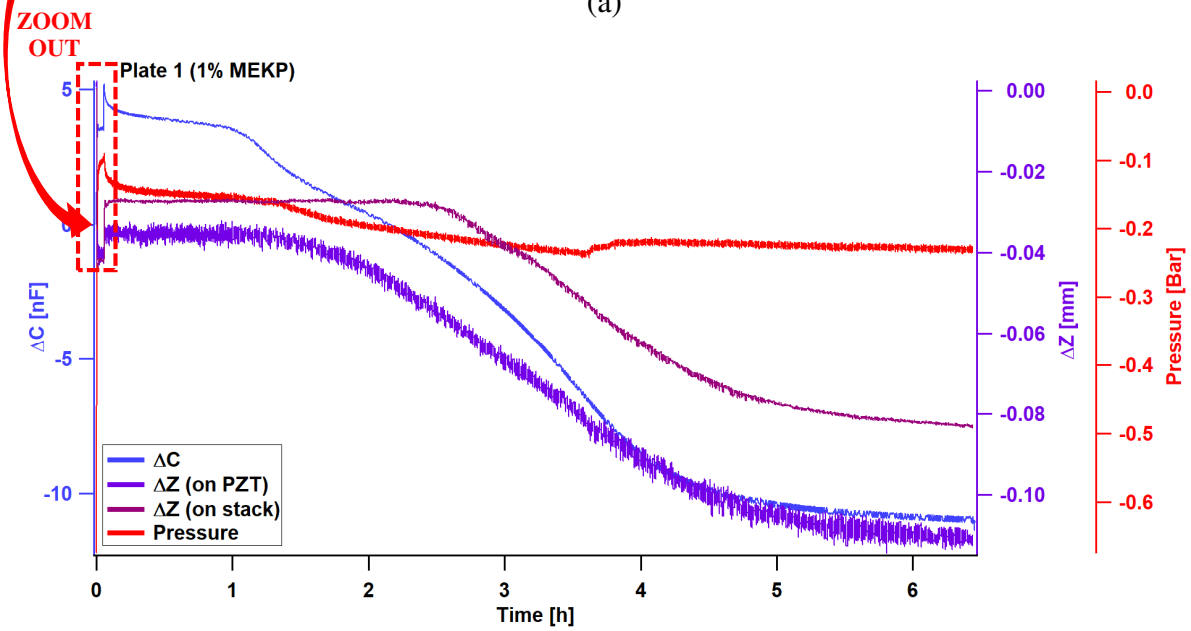

(b) - 1

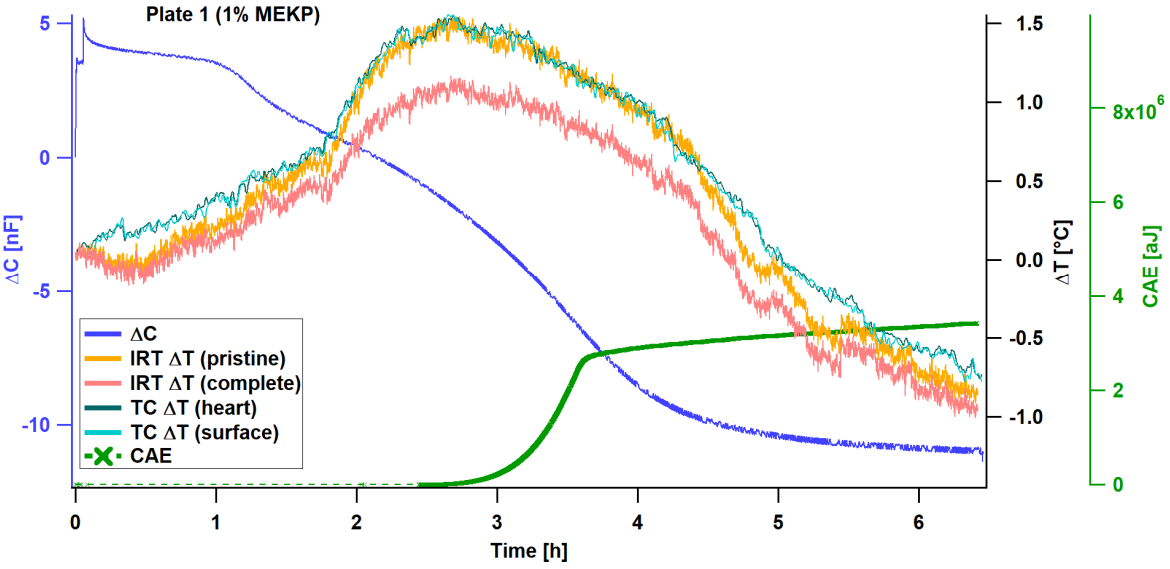

(b) - 2

Figure 5. *Results of the multi-instrumented LRI for a reference PMC plate: (a) injection stage, (b) PZT capacitance variation versus (1) ΔZ & Pressure and (2) ΔT & CAE during full manufacturing*

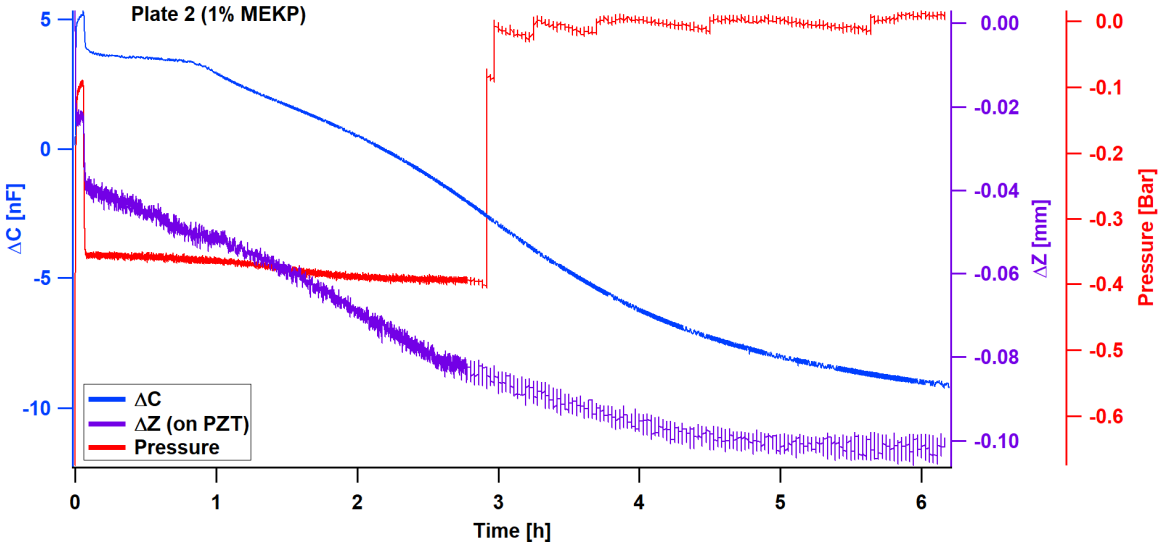

(a)

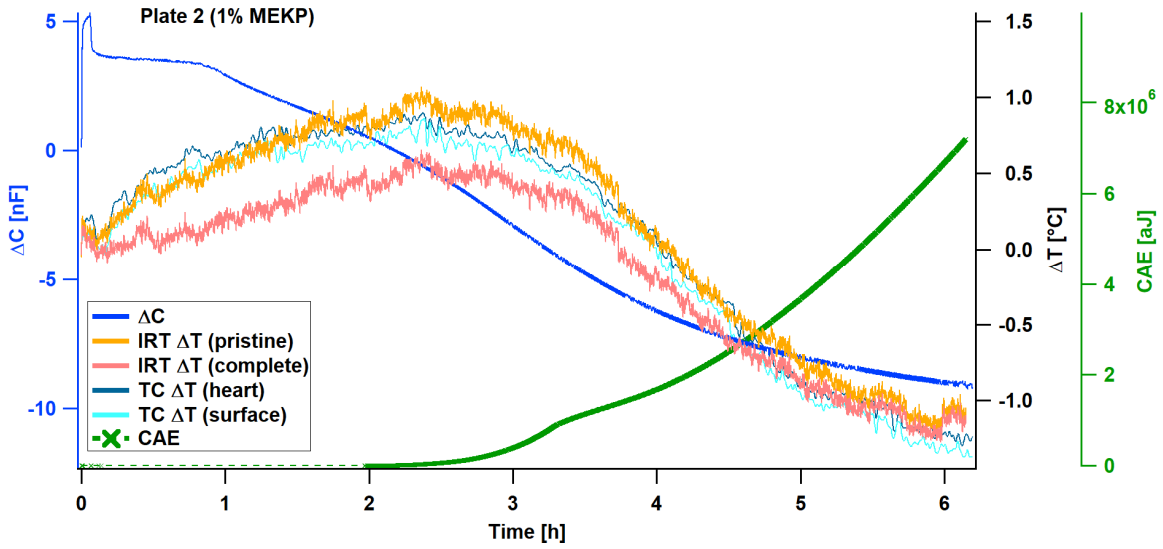

(b)

Figure 6. *Multi-instrumented LRI : 2nd repeatability*

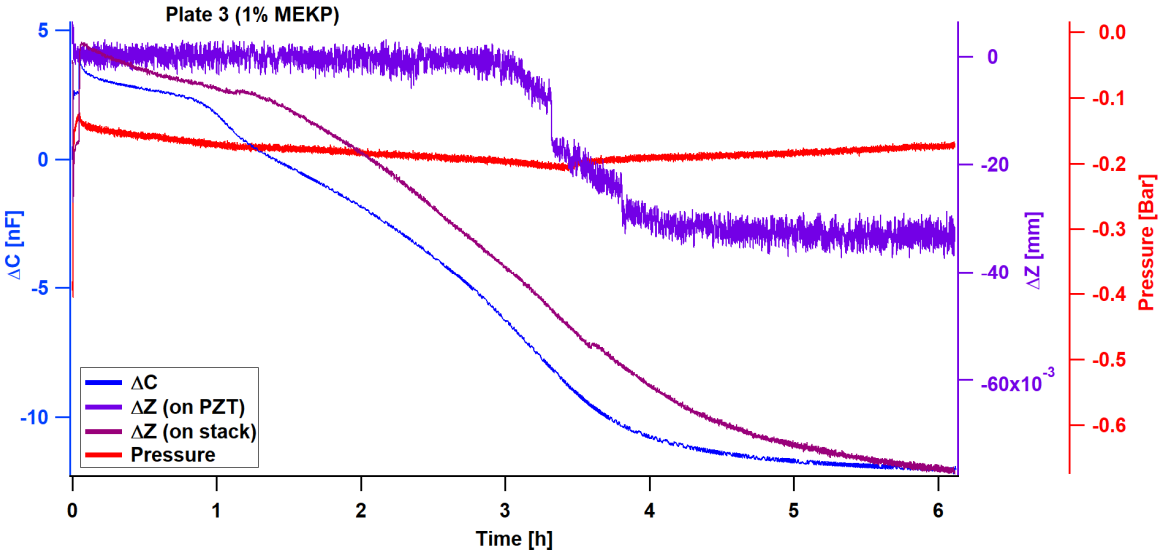

(a)

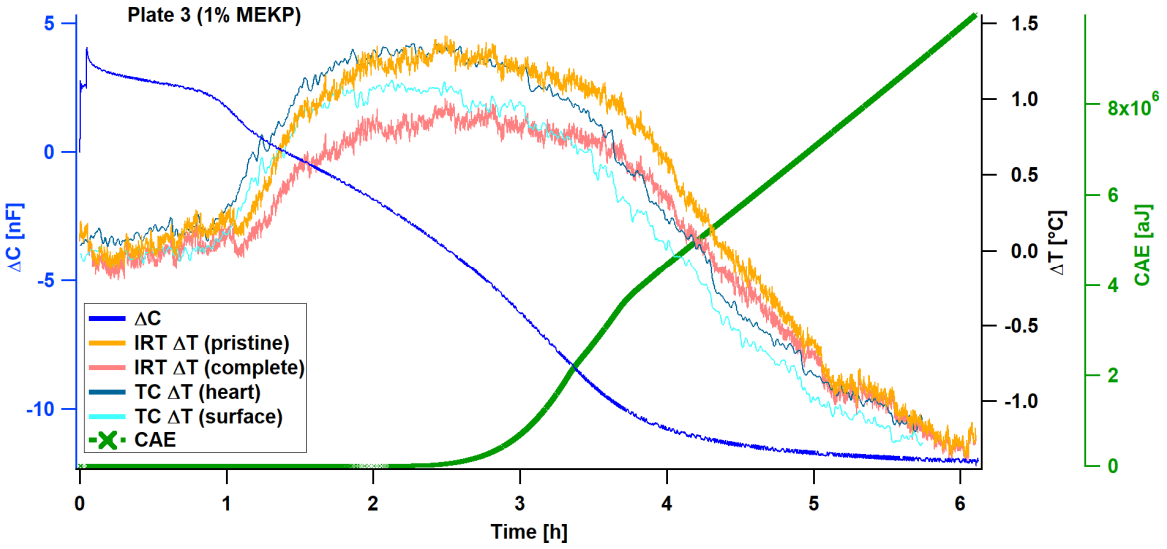

(b)

Figure 7. *Multi-instrumented LRI : 3rd repeatability*

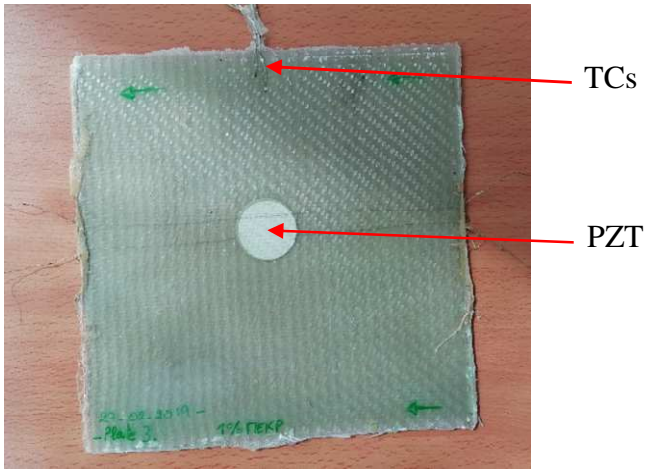

Figure 8. *Typical 150*150*1.3mm^3 glass fiber/polyester composite plate (with in-situ PZT & TCs)*

For the capacitance variation ΔC, a quite chaotic beginning is observed. Looking at a zoom made on this part (**Figure 5** a), which corresponds to the resin injection stage, several steps are defined inside it using correlations obtained between capacitance, pressure and LVDTs signatures. The first part of injection is associated with the increase of both capacitance and pressure signatures. This is due to the arrival of the resin into the dry preform, which progressively releases the in-situ PZT in its environment until full preform impregnation, making its capacitance raise [97], and decreasing the initial depression created by the vacuum pump. After this first part, two important times have been recorded: the ascent of the resin by the output pipe of the system (red line 'A' on **Figure 5** a) corresponding to the point where the preform is fully saturated with resin, and the shutdown of the two taps of the system when finishing the injection part of the infusion process with no more resin flowing (green line 'B' on **Figure 5** a). It is clearly noticeable that 'A' corresponds to a stabilization of the 3

signatures after a first brutal variation: this is associated to the ending of preform impregnation by the resin, which induces some kind of equilibrium state in the system, where the resin only passes through the preform to remove air bubbles still trapped into it. When looking at 'B', a capacitance spike associated to a pressure decrease is noticed, along with a jump in the two LVDT curves. Indeed, the closing of the taps brutally isolated the infusion system from the vacuum pump, which induced a slight swelling of the vacuum bag before it came back to a depression state. This swelling released the PZT sensor a little bit, as well as the LVDTs on the bag, which provoked its momentary increase in capacitance before the bag compressed it again, inducing the stabilization of the bag and thus of LVDT signatures and PZT capacitance. The pressure sensor immediately detected the taps shutdown, with a quick decrease in pressure linked to the fact that there is no more resin flow to oppose the initial depression created into the system by the pump, followed by a stabilization when the pressure equilibrated itself progressively inside the plate.

b. Post-injection stage : resin curing & end of reaction

Looking at **Figure 5** b-1 & b-2, several couplings are noticed between the different in and ex-situ signatures. First of all, it is clear that TC located inside the fiber stack and IRT data taken in the pristine zone are coherent with each other (**Figure 5**b-2), which confirms the ability of IRT to measure temperature variations occurring inside the fiber stack, even if this technique is external. It is however important to perform IRT ΔT ($T\text{-}T_0$) computation using a 'pristine' zone of the plate (small yellow zone in **Figure 3** & yellow curve in **Figure 5**b-2), otherwise the results will be compromised by the obstacles between the zone to measure and the IRT detector (large pink zone in **Figure 3** & pink curve in **Figure 5**b-2). Knowing that, it was decided to trust the IRT camera in the pristine zone, and will not show TCs and IRT (large zone) measurements for the rest of this paper. Continuing with IRT results, two main phenomena are identified during manufacturing: first, a rise of temperature, attributed to the exothermic curing reaction of the resin mixed with the hardener. The second thermal phenomena is the cooling of the infusion system after the temperature apex, which is associated to the end of the curing reaction.

Following the injection stage previously described in 4.1.a, a quasi-constant holding in ΔC is marked, after which the capacitance starts to drop until the end of the experiment. This decrease starting during the rise of IRT ΔT (**Figure 5**b-2) for each plate was supposed to be the PZT being able to detect the beginning of the curing reaction of the resin. Indeed, the more a PZT is constrained in its environment, here due to resin curing contraction, the more its capacitance decreases [97]. The LVDT sensors were placed on the top of the preform to sense the negative Z-displacement of the plate which would be associated to the resin curing contraction, both in the PZT and preform areas. When looking at their signatures variations in **Figure 5**b-1, it is noticeable that they follow the same trends as capacitance does, but their decrease following the plateau happens later. This difference is explained by the nature of the measurement: the capacitance signal is coming from the core of the material because the PZT transducer is in direct contact with the surrounding resin, whereas the LVDT measurements are external and positioned on the vacuum bag. LVDT signatures seem to stabilize long after the IRT ΔT apex and along with the own capacitance final stabilization, which indicates that the whole curing reaction has not completely occurred after the IRT apex. AE activity, plotted in Cumulative Absolute Energy (CAE) form in **Figure 5**b-2, remains negligible from the beginning of resin injection to the exothermal peak. Indeed, during this period, the generated AE hits cannot propagate through the plate to reach the 4 AE sensors implemented on the surface of the stack because the medium attenuates too much the acoustic waves. However, when the exothermal peak is reached, the CAE marks a jump for all PMC plates. This rise reflects a progressive consolidation of the ultrasonic wave propagation medium, with the

sufficient curing level of the resin confirmed by the exothermal peak. This acoustic activity is majorly induced by the vibration of the PZT sensor, as the injected current necessary to measure its capacitance makes it vibrate due to the inverse piezoelectric effect. This is confirmed when looking at the acoustic events location graph presented on **Figure 9**. For each CAE curve, two slopes are detected. As the beginning of the first one coincides with the temperature apex, and the beginning of the second one occurs when the IRT ΔT starts to decrease, they must reflect two different transformation regimes of the matrix. Another remark concerns the quasi constancy of the second CAE slope, which explains that the composite is almost fully cured at that time, giving to the acoustic waves propagation medium quasi constant properties.

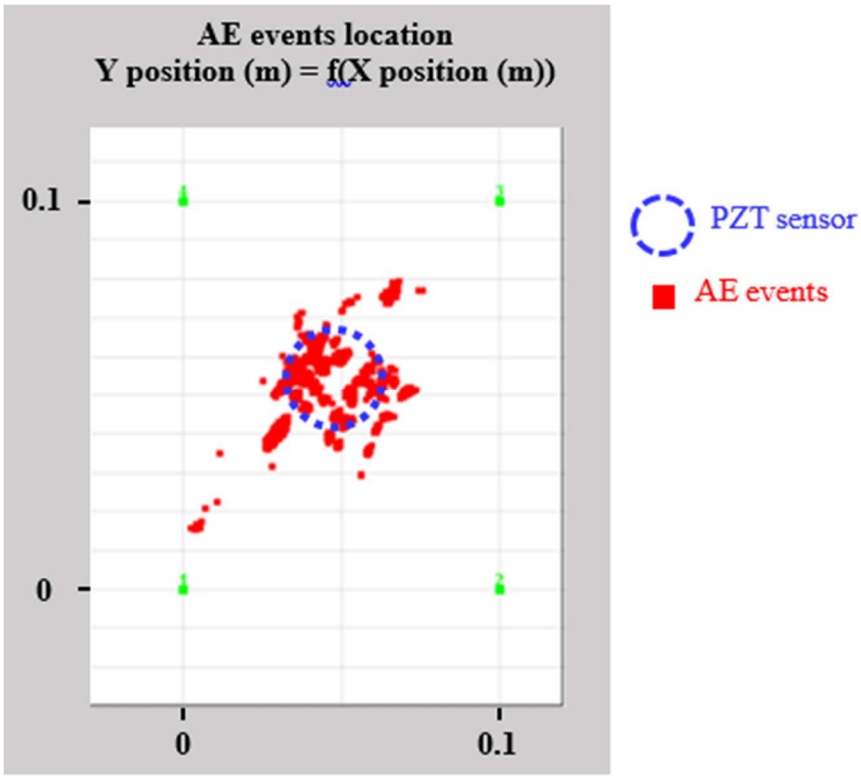

Figure 9. *Location of AE events on a small plate being cured on AEwin software (plate 1)*

Finally, the pressure data (**Figure 5**b-1) are combined to several of the previously interpreted measurements: pressure seems to follow the same trend as capacitance and LVDT do during the whole process. It is clearly noticeable for all plates that with the curing of the resin comes an increasing depression in the infusion system. Another interesting point to highlight is the possibility of the pressure sensor to be isolated from the infusion system if the hole cut out of the vacuum bag on which it is stuck on gets clogged by the cured matrix. This phenomenon has been observed for plate 2 (**Figure 6** a), when the pressure curve suddenly went to 0 bar around 3 hours after resin injection, a little after the IRT ΔT apex.

The interpreted data showed that for each plate, the in-situ PZT sensor was reacting to several stages of the infusion process, such as resin injection and what is supposed to be the curing reaction of the polyester resin mixed with the hardener. Next part focuses on this curing sensitivity.

4.2. Sensitivity of the in-situ PZT to the resin state transitions during curing: linking the capacitance decrease variations with the NDT measurements and the resin chemo-physical characterization

a. Methodology used to identify resin phase transitions

Looking at **Figure 5** b1 & b2, multiple curvature changes can be observed in the decreasing part of the capacitance curve (sky blue curve in **Figure 10a**). Performing first and second derivative of ΔC in this so-called Region Of Interest (ROI) allows to associate these curvature changes with mathematical inflection points, corresponding to second derivative zero passages along with a sign change, or to first derivative local extrema, as presented in **Figure 10 b & c**. Four points can thus be extracted and annotated from (1) to (4) on **Figure 10 c.** The occurrence times of these four mathematical inflection points have been raised and gathered in **Table 4**. These times are considered repeatable for all plates, with a standard deviation below 16%. These observations allowed to suppose that these inflection points are related to chemo-physical transitions happening during the resin curing process and framing different (un)stable states of the resin.

Table 4. *Information on PZT capacitance inflections points for all manufactured plates*

	Plate 1	**Plate 2**	**Plate 3**	**Average value**	**Standard deviation value**
Time at 1st inflection point (h)	0.69	0.59	0.58	0.62	0.06 (9.7%)
Time at 2nd inflection point (h)	1.27	1.06	1.08	1.14	0.11 (9.6%)
Time at 3rd inflection point (h)	1.90	1.46	1.50	1.62	0.25 (15.4%)
Time at 4th inflection point (h)	3.51	3.14	3.19	3.27	0.20 (6.1%)

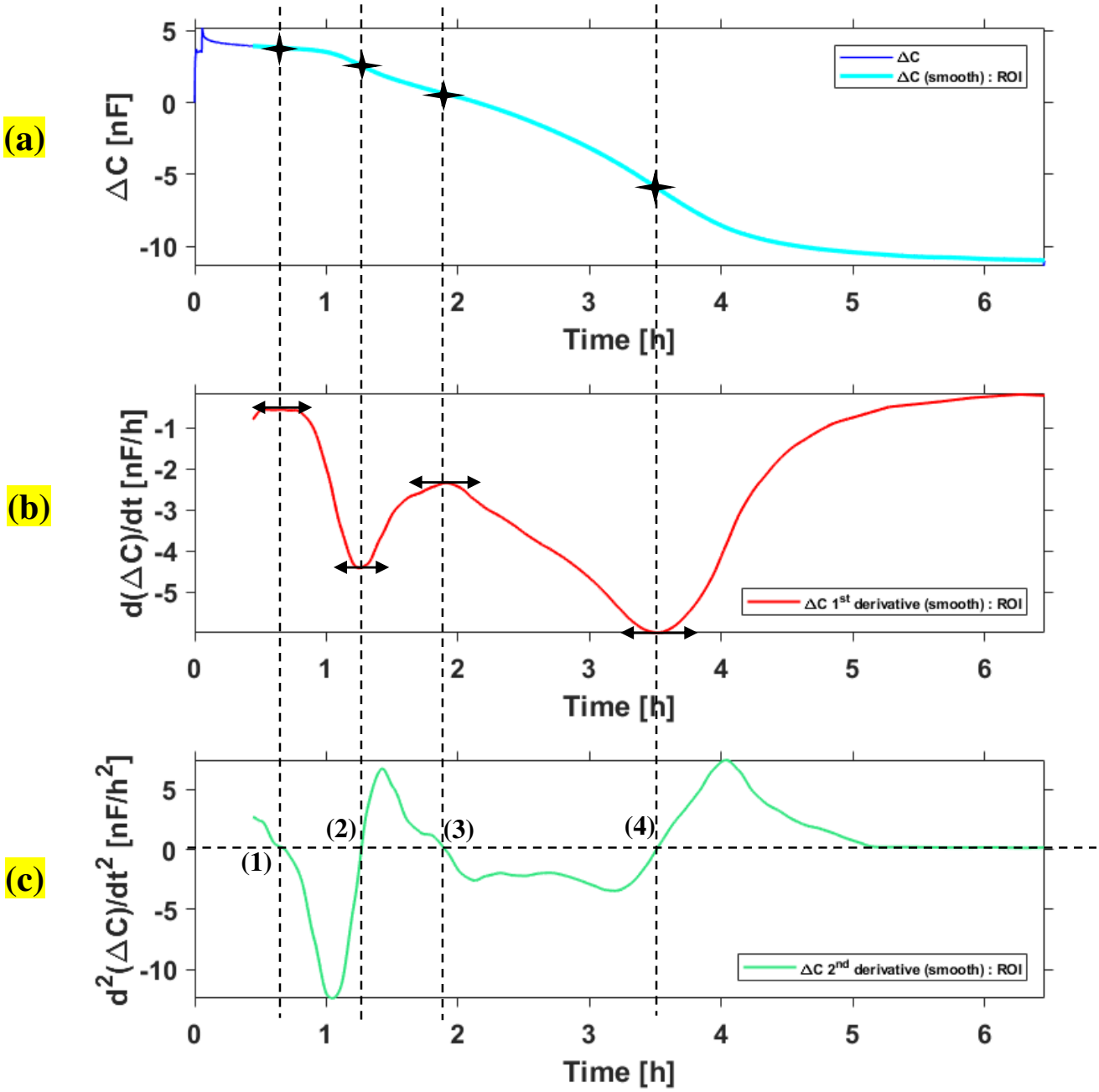

Figure 10. *Methodology used to determine the capacitance inflection points, involving ΔC (a) and its first (b) and second (c) derivatives*

Figure 10 shows the first ΔC inflection point to happen a little before the first ΔC visual decrease mentioned in 4.1.b, and attributed to the beginning of resin curing. The second inflection point seems to be a transition between inflections (1) and (3) when looking at **Figure 10**, and could thus be linked to a regime change inside a chemo-physical transformation, as it cannot be precisely linked to a particular behavior of any of the available NDT data. Concerning the third one, it happens during the IRT ΔT rise towards its apex and not long before the beginning of CAE rise for all manufactured plates. Thus, this inflection corresponds to the initiation of another important change in the chemo-physical structure of the resin. The fourth inflection happens after the final decrease of IRT ΔT from its apex,

around the beginning of the second and quasi-constant slope of acoustic CAE and around the final rise of pressure for all plates. This was attributed to the change toward the quasi-final state of the curing resin, most of the chemical reaction having already occurred. The resin is quasi fully cured, which is also confirmed by the progressive stabilization of LVDT Z-displacements.

The hypotheses emitted on the PZT sensitivity to resin state transitions have been successfully associated with the multi-instrumented infusion data. However, to validate these hypotheses, it was decided to perform chemo-physical characterization tests on the curing resin taken alone and compare the results to those obtained during manufacturing.

b. Identification of the resin phase transitions: links between PZT capacitance variations / NDT signatures & chemo-physical measurements

The idea of this study was to characterize resin gelation and vitrification, as explained in part 3, and correlate them with the various NDT signatures obtained during the performed infusions. As it was not possible to perform real-time chemo-physical characterization of the infusion systems, small resin/hardener samples were tested in oscillatory rheology, even if it was performed apart from the infusions. All the characteristics of the samples are summed up in **Table 3** in section 2. The tests conditions were adapted to mimic infusion process conditions as much as possible, meaning ambient temperature, and angular shear strain γ (1%) and superior plate oscillation frequency (1 Hz) as low as possible to reproduce the stable state of the resin during the whole infusion curing stage. These tests were performed on samples containing the same tested hardener concentration. All the obtained results were normalized with respect to the mass of the corresponding samples, in order to compare them. The rheological tests were performed until the appearance of a viscosity complex modulus stabilization after a continuous increase from the first inflection point, meaning that the curing reaction slowed down a lot. This plateau is assumed to be the end of vitrification, as it is confirmed by the *G''* drop meaning that the cured resin has no remaining viscous properties in its final glassy state. As the three tested rheological samples were repeatable, only curves obtained with sample 1 are shown thereafter, and compared to NDT data obtained with Plate 1. After these tests, correlations were searched between the rheological curves and the ones obtained during the infusion of the different plates, especially in-situ PZT capacitance, IRT ΔT, acoustic emission (CAE) and pressure.

- *Gelation*

When looking at the graphs presented in **Figure 11** a & b, it is possible to associate the first mathematical inflection point of capacitance to the crossing of *G'* and *G''*, meaning gelation (annotation (1) in **Figure 11** a). This confirms that when the resin passes from a liquid state to a rubber state (gel), it starts to compress the PZT transducer and makes its capacitance decrease. At this time, as the resin is under a gel form, no acoustic waves coming from the vibrating PZT can be transmitted to the external AE sensors, making the CAE values null or negligible, as shown in **Figure 11** b. The pressure is also found decreasing due to the progressive solidification of the matrix in the system, which is also the reason of the IRT ΔT rising start in **Figure 11** b. The association of inflection (1) with gelation start is confirmed when looking at the first line of **Table 5**, which displays the good repeatability of rheological measurements with respect to the capacitance first inflection point for the 3 manufactured plates.

- *Vitrification*

The third capacitance inflection point can be associated with resin vitrification at the maximum of the G'' curve (annotation (3) in **Figure 11** a), when looking at the second line of **Table 5**. The gap for Plate 2 and Plate 3 is a little high and can be explained by manufacturing variability, such as variable porosity amount directly impacting the PZT compression by the curing resin. Besides, 30 minutes of gap regarding the 6 hours of manufacturing can be considered acceptable for a transition detection. The found correlation is coherent because the transition from a gel to a (much more rigid) glass makes the resin compress the PZT, which induces a change in its decreasing capacitance slope and thus a new inflection point. At that moment, as previously said above, the IRT ΔT is relatively close to peaking, and the CAE curve is not far from its first rise. This is also relevant because as the curing reaction releases heat, this heat will be close to its maximum when starting the final stage of the curing, that is to say, vitrification. Besides, the resin becoming a glass progressively, it is close to be sufficiently cured and solid to propagate acoustic waves, explaining the CAE rise to come. As the resin is still being cured at this stage, the pressure is still found decreasing.

As previously mentioned in 4.2.a, rheological measurements cannot associate the second capacitance inflection point with a peculiar chemo-physical phenomenon, which seems logical as no intermediate state exists between gelation and vitrification when looking at the literature. Thus, it was decided to associate it with a transition happening at the end of gelation and announcing the beginning of vitrification, and not to mention it on the graphs of **Figure 11**.

- *End of curing reaction*

The fourth and last relevant capacitance inflection point appears more than three hours after the beginning of resin injection. At this time, the *G'* curve has already converged to a final plateau, and the *G''* one has returned to zero (annotation (4) in **Figure 11** a). However, this last inflection always happened at a time the rheological tests never reached, because of the risk of breakage of the rheometer when a too rigid sample is tested too long. *G'* and *G''* behaviors mean that the resin is quasi fully cured at that time, corresponding to the end of vitrification, which is the final curing stage. Indeed, as a solid glass, the resin has only an elastic behavior and no remaining viscous properties at that time. This last inflection point occurs around the previously noticed change of CAE slope to a quasi-linear behavior, which confirms the hypothesis that at this time, the acoustic waves propagation medium has acquired almost constant properties (**Figure 11** b). It is also well-correlated with the IRT ΔT fall after the exothermal peak (**Figure 11** b) because as the reaction ends, no more heat is released, and happens not far from a final pressure rise and stabilization, illustrated in **Figure 5** b-1, **Figure 6** a and **Figure 7** a. This pressure behavior corresponds to the partial (or complete in case of plate 2) clogging of the cut-out connection hole made inside the vacuum bag by the vitrified resin. It is, however, relevant to point out that after the appearance of the fourth capacitance inflection point, the corresponding signal is still decreasing, which means that the curing reaction, even almost finished, is still ongoing. Only remains the curing of a very few resin percentages. To sum up this part, it is now possible to associate each of the three relevant capacitance inflection points with the beginning of a chemo-physical transformation of the curing matrix: gelation, vitrification and finally the slow curing of a small residual resin amount after the end of vitrification.

Table 5. *Gap between mean rheological values taken on 3 samples and Capacitance inflection points (1) & (3)*

	Plate 1	**Plate 2**	**Plate 3**

G'/G" crossing time: Gelation (min)	0.22 (inflection 1)	6.46 (inflection 1)	8.14 (inflection 1)
Maximum G" time: Vitrification (min)	8.55 (inflection 3)	36.07 (inflection 3)	34.57 (inflection 3)

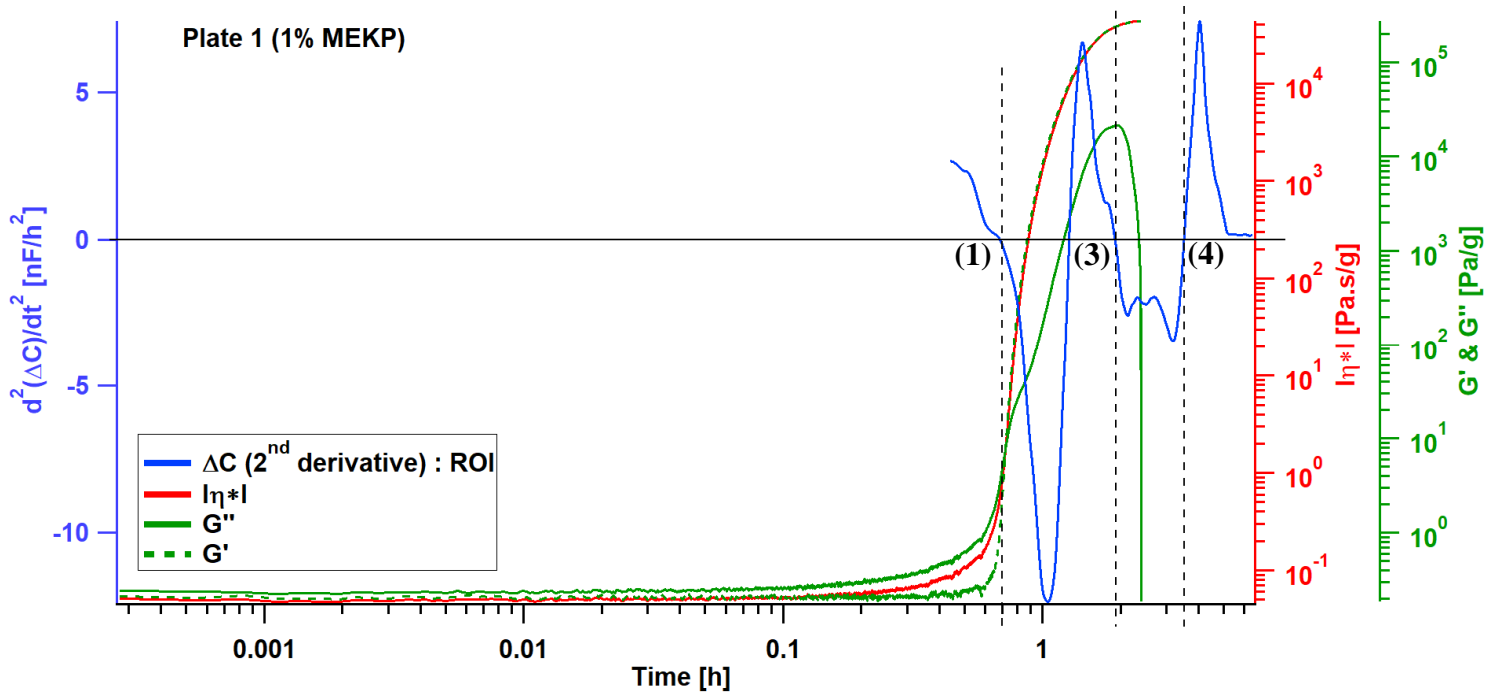

(a)

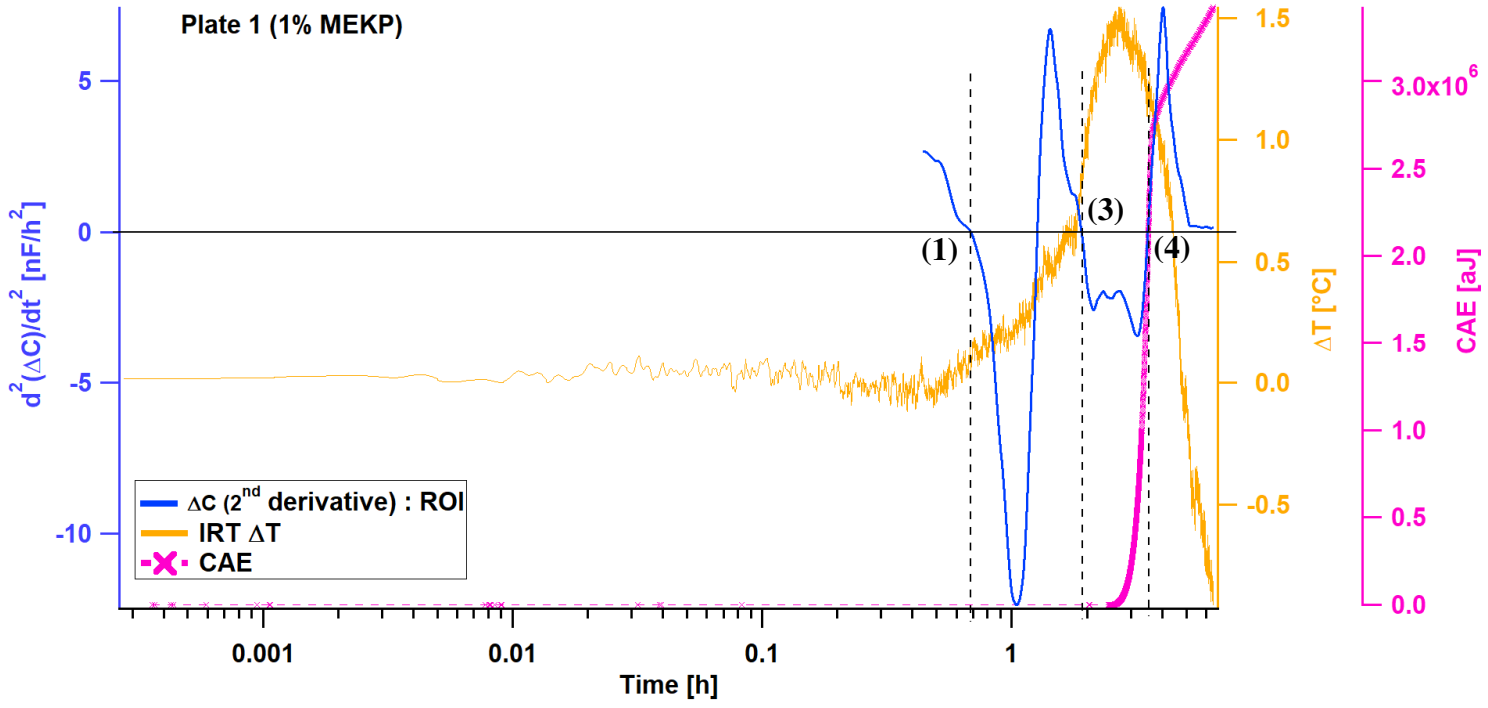

(b)

Figure 11. *Comparison of ΔC second derivative for Plate 1 with: (a) rheological measurements and (b) ΔT & Cumulative Absolute Energy of AE hits*

5. Conclusions and outlooks

In this work, the interest of embedding a thin piezoceramic disc sensor inside a PMC preform to perform in-situ and real-time PM of the infusion manufacturing is investigated. Several internal and external NDT instrumentations are implemented to make correlations between the different obtained measurements. Multiple couplings are illustrated between the different signatures, providing information about both preform impregnation and resin curing after injection. The capacitance variation of the in-situ PZT illustrates 3 relevant inflection points during its decreasing variation (ROI), and these ones were investigated thanks to the multi-instrumentation data and rheological measurements performed aside on pure resin + hardener samples. These new tests allowed to associate the first inflection point to resin gelation beginning, the second one to its vitrification beginning, and the third one to the curing of the few last remaining resin percentages after the end of vitrification. The potential of this embedded PZT transducer, which gives repeatable and relatively accurate information about different essential transitions happening during the whole process, is obvious. The end of vitrification corresponding to the last capacitance inflection point (n°4 on the previous graphs) is of particular interest, as it can be used industrially to know the time when the composite parts can be demolded without major risks, and thus improve production rates: LRI being one of the most time-consuming manufacturing method in composite materials industry, this time saving would be highly appreciable. This vitrification information will also be of particular interest for LCM processes using closed molds, such as RTM, where there is no possibility to retrieve visual information about the manufacturing progress. It would allow to know in which step of the curing process the manufactured part is, and thus when to demold the plate without the need to see or touch it. This work used glass fiber as a cheap reinforcing material, but the study remains applicable on carbon fiber preforms used for high-tech industries such as aeronautics or aerospace wherein the PM of high-performance Carbon Fiber Reinforced Polymer (CFRP) parts is a great requirement. The major particularity studying the carbon preforms resides on the insulation of the PZT discs and their connection wires from the surrounding conductive carbon fibers in order to prevent a short circuit. This research also showed the interest of the multi-instrumentation to monitor the process in real-time. Particularly, the tandem formed by the in-situ PZT disc and the 4 external AE sensors creates an A-US system which allows to know when the resin becomes cured enough to transmit acoustic waves as vitrification already began, and when it acquired quasi-constant properties as the cure is almost finished. The final interest is that as the inserted PZT remains operational after the demolding stage, it can also be employed to perform in-situ and real-time SHM of the plate when submitted to various physical loadings, as it is the case during the life in service of a composite structure working in high-tech industries. To do so, the PZT must, of course, be declared non-intrusive in the first place, which means that it will not threaten the operation of its host composite structure during service: no mechanical properties tremendous degradation, no lifetime reduction, or no raised fatigue sensitivity. Finding thresholds to know when to repair or replace them without necessitating usual external and cumbersome SHM techniques would be a significant advance in composite industries.

References

[1] Konstantopoulos S, Fauster E, Schledjewski R. Monitoring the production of FRP composites: A review of in-line sensing methods. Express Polym Lett 2014;8:823–40. doi:10.3144/expresspolymlett.2014.84.

[2] Marin E, Robert L, Triollet SS, Ouerdane Y. Liquid Resin Infusion process monitoring with superimposed Fibre Bragg Grating sensor. Polym Test 2012;31:1045–52. doi:10.1016/j.polymertesting.2012.07.018.

[3] Lee DG, Kim HG. Non-isothermal in situ dielectric cure monitoring for thermosetting matrix composites. J Compos Mater 2004. doi:10.1177/0021998304040563.

[4] Hegg MC, Ogale A, Mescher A, Mamishev A V., Minaie B. Remote monitoring of resin transfer molding processes by distributed dielectric sensors. J Compos Mater 2005. doi:10.1177/0021998305051083.

[5] Yenilmez B, Murat Sozer E. A grid of dielectric sensors to monitor mold filling and resin cure in resin transfer molding. Compos Part A Appl Sci Manuf 2009. doi:10.1016/j.compositesa.2009.01.014.

[6] Kim SS, Murayama H, Kageyama K, Uzawa K, Kanai M. Study on the curing process for carbon/epoxy composites to reduce thermal residual stress. Compos Part A Appl Sci Manuf 2012;43:1197–202. doi:10.1016/j.compositesa.2012.02.023.

[7] Kobayashi S, Matsuzaki R, Todoroki A. Multipoint cure monitoring of CFRP laminates using a flexible matrix sensor. Compos Sci Technol 2009;69:378–84. doi:10.1016/j.compscitech.2008.10.029.

[8] Yang Y, Chiesura G, Vervust T, Bossuyt F, Luyckx G, Degrieck J, et al. Design and fabrication of a flexible dielectric sensor system for in situ and real-time production monitoring of glass fibre reinforced composites. Sensors Actuators, A Phys 2016;243:103–10. doi:10.1016/j.sna.2016.03.015.

[9] Lawrence JM, Hsiao KT, Don RC, Simacek P, Estrada G, Sozer EM, et al. An approach to couple mold design and on-line control to manufacture complex composite parts by resin transfer molding. Compos - Part A Appl Sci Manuf 2002. doi:10.1016/S1359-835X(02)00043-X.

[10] Luthy T, Ermanni P. Flow Monitoring in Liquid Composite Molding Based on Linear Direct Current Sensing Technique. Polym. Compos., 2003. doi:10.1002/pc.10026.

[11] Danisman M, Tuncol G, Kaynar A, Sozer EM. Monitoring of resin flow in the resin transfer molding (RTM) process using point-voltage sensors. Compos Sci Technol 2007. doi:10.1016/j.compscitech.2006.09.011.

[12] Garschke C, Weimer C, Parlevliet PP, Fox BL. Out-of-autoclave cure cycle study of a resin film infusion process using in situ process monitoring. Compos Part A Appl Sci Manuf 2012;43:935–44. doi:10.1016/j.compositesa.2012.01.003.

[13] Hsiao KT. Embedded single carbon fibre to sense the thermomechanical behavior of an epoxy during the cure process. Compos Part A Appl Sci Manuf 2013. doi:10.1016/j.compositesa.2012.11.007.

[14] Pandey G, Deffor H, Thostenson ET, Heider D. Smart tooling with integrated time domain reflectometry sensing line for non-invasive flow and cure monitoring during composites manufacturing. Compos Part A Appl Sci Manuf 2013. doi:10.1016/j.compositesa.2012.11.017.

[15] Dominauskas A, Heider D, Gillespie JW. Electric time-domain reflectometry sensor for online flow sensing in liquid composite molding processing. Compos Part A Appl Sci Manuf 2003. doi:10.1016/S1359-835X(02)00232-4.

[16] Dominauskas A, Heider D, Gillespie JW. Electric time-domain reflectometry distributed flow sensor. Compos Part A Appl Sci Manuf 2007. doi:10.1016/j.compositesa.2006.01.019.

[17] Urabe K, Okabe T, Tsuda H. Monitoring of resin flow and cure with an electromagnetic wave transmission line using carbon fiber as conductive elements. Compos Sci Technol 2002. doi:10.1016/S0266-3538(02)00047-7.
[18] Buchmann C, Filsinger J, Ladstätter E. Investigation of Electrical Time Domain Reflectometry for infusion and cure monitoring in combination with electrically conductive fibers and tooling materials. Compos Part B Eng 2016;94:389–98. doi:10.1016/j.compositesb.2016.02.060.
[19] Kuang KSC, Zhang L, Cantwell WJ, Bennion I. Process monitoring of aluminum-foam sandwich structures based on thermoplastic fibre–metal laminates using fibre Bragg gratings. Compos Sci Technol 2005;65:1800–7. doi:10.1016/j.compscitech.2005.03.009.
[20] Jung K, Kang TJ. Cure monitoring and internal strain measurement of 3-D hybrid braided composites using fiber bragg grating sensor. J Compos Mater 2007. doi:10.1177/0021998306068088.
[21] Khoun L, De Oliveira R, Michaud V, Hubert P. Investigation of process-induced strains development by fibre Bragg grating sensors in resin transfer moulded composites. Compos Part A Appl Sci Manuf 2011;42:274–82. doi:10.1016/j.compositesa.2010.11.013.
[22] Archer E, Broderick J, McIlhagger AT. Internal strain measurement and cure monitoring of 3D angle interlock woven carbon fibre composites. Compos Part B Eng 2014. doi:10.1016/j.compositesb.2013.08.067.
[23] Tsai L, Cheng T-C, Lin C-L, Chiang C-C. Application of the embedded optical fiber Bragg grating sensors in curing monitoring of Gr/epoxy laminated composites. Smart Sens Phenomena, Technol Networks, Syst 2009 2009;7293:729307. doi:10.1117/12.817520.
[24] Samet N, Maréchal P, Duflo H. Ultrasonic characterization of a fluid layer using a broadband transducer. Ultrasonics 2012;52:427–34. doi:10.1016/j.ultras.2011.10.004.
[25] Ghodhbani N, Maréchal P, Duflo H. Ultrasound monitoring of the cure kinetics of an epoxy resin: Identification, frequency and temperature dependence. Polym Test 2016;56:156–66. doi:10.1016/j.polymertesting.2016.10.009.
[26] Schmachtenberg E, Schulte Zur Heide J, Töpker J. Application of ultrasonics for the process control of Resin Transfer Moulding (RTM). Polym Test 2005. doi:10.1016/j.polymertesting.2004.11.002.
[27] Visvanathan K, Balasubramaniam K. Ultrasonic torsional guided wave sensor for flow front monitoring inside molds. Rev Sci Instrum 2007. doi:10.1063/1.2432258.
[28] Pavlopoulou S, Soutis C, Staszewski WJ. Cure monitoring through time–frequency analysis of guided ultrasonic waves. Plast Rubber Compos 2012. doi:10.1179/1743289811y.0000000052.
[29] Liebers N, Raddatz F, Schadow F. Effective and flexible ultrasound sensors for cure monitoring for industrial composites production. Dtsch. Luft- und Raumfahrtkongress 2012, 2012.
[30] Lin M, Chang F-K. Composite structures with built-in diagnostics. Mater Today 1999;2:18–22. doi:10.1016/S1369-7021(99)80007-8.
[31] Lin M, Chang FK. The manufacture of composite structures with a built-in network of piezoceramics. Compos Sci Technol 2002;62:919–39. doi:10.1016/S0266-3538(02)00007-6.
[32] Chilles JS, Koutsomitopoulou AF, Croxford AJ, Bond IP. Monitoring cure and detecting damage in composites with inductively coupled embedded sensors. Compos Sci Technol 2016;134:81–8. doi:10.1016/j.compscitech.2016.07.028.
[33] Ghodhbani N, Marechal P, Duflo H. Ultrasonic broadband characterization of a viscous

liquid: Methods and perturbation factors. Ultrasonics 2015;56:308–17. doi:10.1016/j.ultras.2014.08.013.
[34] Kline R, Parasnis N, Konanur R. Ultrasonic monitoring of the dynamic properties of composites during manufacture. Ultrason Symp 1992;9:0–87.
[35] Samet N, Maréchal P, Duflo H. Ultrasound monitoring of bubble size and velocity in a fluid model using phased array transducer. NDT E Int 2011;44:621–7. doi:10.1016/j.ndteint.2011.06.005.
[36] Samet N, Marechal P, Duflo H. Monitoring of an ascending air bubble in a viscous fluid/fiber matrix medium using a phased array transducer. Eur J Mech B/Fluids 2015;54:45–52. doi:10.1016/j.euromechflu.2015.06.012.
[37] Fomitchov PA, Kim YK, Kromine AK, Krishnaswamy S. Laser ultrasonic array system for real-time cure monitoring of polymer-matrix composites. J Compos Mater 2002. doi:10.1177/0021998302036015245.
[38] Wang P, Molimard J, Drapier S, Vautrin A, Minni JC. Monitoring the resin infusion manufacturing process under industrial environment using distributed sensors. J Compos Mater 2012;46:691–706. doi:10.1177/0021998311410479.
[39] Lekakou C, Cook S, Deng Y, Ang TW, Reed GT. Optical fibre sensor for monitoring flow and resin curing in composites manufacturing. Compos. Part A Appl. Sci. Manuf., 2006. doi:10.1016/j.compositesa.2005.03.003.
[40] Li C, Cao M, Wang R, Wang Z, Qiao Y, Wan L, et al. Fiber-optic composite cure sensor: Monitoring the curing process of composite material based on intensity modulation. Compos Sci Technol 2003;63:1749–58. doi:10.1016/S0266-3538(03)00118-0.
[41] Gupta N, Sundaram R. Fiber optic sensors for monitoring flow in vacuum enhanced resin infusion technology (VERITy) process. Compos Part A Appl Sci Manuf 2009;40:1065–70. doi:10.1016/j.compositesa.2009.04.022.
[42] Buggy SJ, Chehura E, James SW, Tatam RP. Optical fibre grating refractometers for resin cure monitoring. J Opt A Pure Appl Opt 2007. doi:10.1088/1464-4258/9/6/S09.
[43] Milkovich S, Altkorn R, Haidle R, Neatrour MJ, Fildes JM. In Situ Sensors for Intelligent Process Control for Fabrication of Polymer-Matrix Composite Materials. vol. 2191, 1994, p. 349–60.
[44] Wang L, Pandita S, Machavaram VR, Malik S, Harris D, Fernando GF. Characterisation of the cross-linking process in an E-glass fibre/epoxy composite using evanescent wave spectroscopy. Compos Sci Technol 2009;69:2069–74. doi:10.1016/j.compscitech.2008.11.001.
[45] Dunkers JP, Lenhart JL, Kueh SR, Van Zanten JH, Advani SG, Parnas RS. Fiber optic flow and cure sensing for liquid composite molding. Opt Lasers Eng 2001. doi:10.1016/S0143-8166(00)00110-X.
[46] Wood KH, Brown TL, Wu MC, Gause CB, Wood K. H., Brown TL, et al. Fiber optic sensors for cure/health monitoring of composite materials 2004.
[47] Anne ML, Salle ELG La, Bureau B, Tristant J, Brochot F, Boussard-Plédel C, et al. Polymerisation of an industrial resin monitored by infrared fiber evanescent wave spectroscopy. Sensors Actuators, B Chem 2009. doi:10.1016/j.snb.2009.01.069.
[48] Cruz JC, Osswald TA. Monitoring epoxy and unsaturated polyester reactions under pressure-reaction rates and mechanical properties. Polym Eng Sci 2009. doi:10.1002/pen.21448.
[49] Lee CW. Monitoring of Epoxy / Graphite Composites Using a Scaling Analysis and a Dual Heat Flux Sensor On-Line Cure. J Compos Mater 1991:274–92.
[50] Hsiao KT, Little R, Restrepo O, Minaie B. A study of direct cure kinetics characterization during liquid composite molding. Compos. Part A Appl. Sci. Manuf.,

2006. doi:10.1016/j.compositesa.2005.01.019.
[51] Tuncol G, Danisman M, Kaynar A, Sozer EM. Constraints on monitoring resin flow in the resin transfer molding (RTM) process by using thermocouple sensors. Compos Part A Appl Sci Manuf 2007. doi:10.1016/j.compositesa.2006.10.009.
[52] Yoon HJ, Costantini DM, Limberger HG, Salathé RP, Kim CG, Michaud V. In situ strain and temperature monitoring of adaptive composite materials. J Intell Mater Syst Struct 2006. doi:10.1177/1045389X06064889.
[53] Cuevas E, García C, Hernandez S, Gomez T, Cañada M. Non destructive testing for non cured composites: Air coupled Ultrasounds and Thermography. 5th Int. Symp. NDT Aerosp., 2013.
[54] Wang P, Drapier S, Molimard J, Vautrin A, Minni JC. Characterization of Liquid Resin Infusion (LRI) filling by fringe pattern projection and in situ thermocouples. Compos Part A Appl Sci Manuf 2010;41:36–44. doi:10.1016/j.compositesa.2009.09.007.
[55] Leonard-Williams S. The crossover from RTM to resin infusion. Reinf Plast 2008;52:28–9. doi:10.1016/S0034-3617(08)70371-0.
[56] Di Fratta C, Klunker F, Ermanni P. A methodology for flow-front estimation in LCM processes based on pressure sensors. Compos Part A Appl Sci Manuf 2013. doi:10.1016/j.compositesa.2012.11.008.
[57] Govignon Q, Bickerton S, Kelly PA. Experimental investigation into the post-filling stage of the resin infusion process. J Compos Mater 2013. doi:10.1177/0021998312448500.
[58] Xin C, Gu Y, Li M, Li Y, Zhang Z. Online monitoring and analysis of resin pressure inside composite laminate during zero-bleeding autoclave process. Polym Compos 2011. doi:10.1002/pc.21048.
[59] Simacek P, Eksik Ö, Heider D, Gillespie JW, Advani S. Experimental validation of post-filling flow in vacuum assisted resin transfer molding processes. Compos Part A Appl Sci Manuf 2012. doi:10.1016/j.compositesa.2011.10.002.
[60] Kobayashi S, Tanaka A, Morimoto T. Analytical prediction of resin impregnation behavior during processing of unidirectional fiber reinforced thermoplastic composites considering pressure fluctuation. Adv Compos Mater 2012. doi:10.1080/09243046.2012.740773.
[61] Vilà J, González C, Llorca J. A level set approach for the analysis of flow and compaction during resin infusion in composite materials. Compos Part A Appl Sci Manuf 2014;67:299–307. doi:10.1016/j.compositesa.2014.09.002.
[62] Yenilmez B, Senan M, Murat Sozer E. Variation of part thickness and compaction pressure in vacuum infusion process. Compos Sci Technol 2009;69:1710–9. doi:10.1016/j.compscitech.2008.05.009.
[63] Timms J, Bickerton S, Kelly PA. Laminate thickness and resin pressure evolution during axisymmetric liquid composite moulding with flexible tooling. Compos Part A Appl Sci Manuf 2012;43:621–30. doi:10.1016/j.compositesa.2011.12.012.
[64] Hautefeuille A, Comas-Cardona S, Binetruy C. Mechanical signature and full-field measurement of flow-induced large in-plane deformation of fibrous reinforcements in composite processing. Compos Part A Appl Sci Manuf 2019;118:213–22. doi:10.1016/j.compositesa.2018.12.030.
[65] Gourichon B, Binetruy C, Krawczak P. Experimental investigation of high fiber tow count fabric unsaturation during RTM. Compos Sci Technol 2006;66:976–82. doi:10.1016/j.compscitech.2005.07.032.
[66] Matsuzaki R, Kobayashi S, Todoroki A, Mizutani Y. Cross-sectional monitoring of resin impregnation using an area-sensor array in an RTM process. Compos Part A Appl Sci Manuf 2012;43:695–702. doi:10.1016/j.compositesa.2011.12.024.

[67] Murata M, Matsuzaki R, Todoroki A, Mizutani Y, Suzuki Y. Three-dimensional reconstruction of resin flow using capacitance sensor data assimilation during a liquid composite molding process: A numerical study. Compos Part A Appl Sci Manuf 2015;73:1–10. doi:10.1016/j.compositesa.2015.01.031.
[68] Lu S, Chen D, Wang X, Shao J, Ma K, Zhang L, et al. Real-time cure behaviour monitoring of polymer composites using a highly flexible and sensitive CNT buckypaper sensor. Compos Sci Technol 2017. doi:10.1016/j.compscitech.2017.09.025.
[69] Kahali Moghaddam M, Breede A, Chaloupka A, Bödecker A, Habben C, Meyer EM, et al. Design, fabrication and embedding of microscale interdigital sensors for real-time cure monitoring during composite manufacturing. Sensors Actuators, A Phys 2016;243:123–33. doi:10.1016/j.sna.2016.03.017.
[70] Mounkaila M. Analyse impédancemétrique pour le suivi de cuisson ou de santé des structures composites carbone/époxyde : Vers des matériaux intelligents pour le PHM des structures composites. 2016.
[71] Polanský R, Pihera J, Komárek J, Pavlica R, Prosr P, Freisleben J, et al. Development of a measuring system for on-line in situ monitoring of composite materials manufacturing. Compos Part A Appl Sci Manuf 2016;90:760–70. doi:10.1016/j.compositesa.2016.09.006.
[72] Saint-Pierre N, Perrissin-Fabert I, Jayet Y, Tatibouet J. MONITORING THE HYDROLYTIC DEGRADATION OF POLYESTER-BASED COMPOSITES BY A PIEZOELECTRIC METHOD. J Reinf Plast Compos 1996.
[73] May D, Aktas A, Advani SG, Berg DC, Endruweit A, Fauster E, et al. In-Plane Permeability Characterization of Engineering Textiles Based On Radial Flow Experiments: A Benchmark Exercise. Compos Part A Appl Sci Manuf 2019;121:100–14. doi:10.1016/j.compositesa.2019.03.006.
[74] Hoes K, Dinescu D, Sol H, Vanheule M, Parnas RS, Luo Y, et al. New set-up for measurement of permeability properties of fibrous reinforcements for RTM. Compos - Part A Appl Sci Manuf 2002;33:959–69. doi:10.1016/S1359-835X(02)00035-0.
[75] Bancora SP, Binetruy C, Advani SG, Syerko E, Comas-Cardona S. Effective permeability averaging scheme to address in-plane anisotropy effects in multi-layered preforms. Compos Part A Appl Sci Manuf 2018;113:359–69. doi:10.1016/j.compositesa.2018.07.025.
[76] Canal LP, Benavente M, Hausmann M, Michaud V. Process-induced strains in RTM processing of polyurethane/carbon composites. Compos Part A Appl Sci Manuf 2015;78:264–73. doi:10.1016/j.compositesa.2015.08.018.
[77] Chandarana N, Martinez-Sanchez D, Soutis C, Gresil M. Early Damage Detection in Composites by Distributed Strain and Acoustic Event Monitoring. Procedia Eng 2017;188:88–95. doi:10.1016/j.proeng.2017.04.515.
[78] Sánchez DM, Gresil M, Soutis C. Distributed internal strain measurement during composite manufacturing using optical fibre sensors. Compos Sci Technol 2015;120:49–57. doi:10.1016/j.compscitech.2015.09.023.
[79] Parlevliet PP, Voet E, Bersee HEN, Beukers A. Process monitoring with fbg sensors during vacuum infusion of thick composite laminates. ICCM Int Conf Compos Mater 2007.
[80] Ali MA, Umer R, Khan KA, Samad YA, Liao K, Cantwell W. Graphene coated piezo-resistive fabrics for liquid composite molding process monitoring. Compos Sci Technol 2017;148:106–14. doi:10.1016/j.compscitech.2017.05.022.
[81] Park JM, Lee S Il, Choi JH. Cure monitoring and residual stress sensing of single-carbon fiber reinforced epoxy composites using electrical resistivity measurement.

Compos Sci Technol 2005;65:571–80. doi:10.1016/j.compscitech.2004.09.019.
[82] Luo S, Wang G, Wang Y, Xu Y, Luo Y. Carbon nanomaterials enabled fiber sensors: A structure-oriented strategy for highly sensitive and versatile in situ monitoring of composite curing process. Compos Part B Eng 2019;166:645–52. doi:10.1016/j.compositesb.2019.02.067.
[83] Gnidakouong JRN, Roh HD, Kim JH, Park Y Bin. In situ process monitoring of hierarchical micro-/nano-composites using percolated carbon nanotube networks. Compos Part A Appl Sci Manuf 2016;84:281–91. doi:10.1016/j.compositesa.2016.01.017.
[84] Modi D, Correia N, Johnson M, Long A, Rudd C, Robitaille F. Active control of the vacuum infusion process. Compos Part A Appl Sci Manuf 2007;38:1271–87. doi:10.1016/j.compositesa.2006.11.012.
[85] Kazilas MC, Partridge IK. Exploring equivalence of information from dielectric and calorimetric measurements of thermoset cure-a model for the relationship between curing temperature, degree of cure and electrical impedance. Polymer (Guildf) 2005;46:5868–78. doi:10.1016/j.polymer.2005.05.005.
[86] Baran I, Akkerman R, Hattel JH. Material characterization of a polyester resin system for the pultrusion process. Compos Part B Eng 2014;64:194–201. doi:10.1016/j.compositesb.2014.04.030.
[87] Chiacchiarelli LM, Kenny JM, Torre L. Kinetic and chemorheological modeling of the vitrification effect of highly reactive poly(urethane-isocyanurate) thermosets. Thermochim Acta 2013;574:88–97. doi:10.1016/j.tca.2013.08.011.
[88] Harizi W, Chaki S, Bourse G, Ourak M. Mechanical damage characterization of glass fiber-reinforced polymer laminates by ultrasonic maps. Compos Part B Eng 2015;70:131–7. doi:10.1016/j.compositesb.2014.11.014.
[89] Martins AT, Aboura Z, Harizi W, Laksimi A, Khellil K. Structural health monitoring for GFRP composite by the piezoresistive response in the tufted reinforcements. Compos Struct 2018;209:103–11. doi:10.1016/j.compstruct.2018.10.091.
[90] Hamdi K, Aboura Z, Harizi W, Khellil K. Improvement of the electrical conductivity of carbon fiber reinforced polymer by incorporation of nanofillers and the resulting thermal and mechanical behavior. J Compos Mater 2017:002199831772658. doi:10.1177/0021998317726588.
[91] Abusrea MR, Arakawa K. Enhanced tensile strength CFRP adhesive joint constructed from carbon fiber-reinforced plastic and dry carbon fiber laminates. Proc 17th Int Conf Compos Mater (ICCM17) 2016.
[92] Kazilas MC. Acquisition and Interpretation of Dielectric Data For Thermoset Cure Monitoring. 2003.
[93] Winter HH, Chambon F. Analysis of Linear Viscoelasticity of a Crosslinking Polymer at the Gel Point. J Rheol (N Y N Y) 1986;30:367–82. doi:10.1122/1.549853.
[94] Haider M, Hubert P, Lessard L. Cure shrinkage characterization and modeling of a polyester resin containing low profile additives 2007;38:994–1009. doi:10.1016/j.compositesa.2006.06.020.
[95] Dev S, Shah PN, Zhang Y, Ryan D, Hansen CJ, Lee Y. Synthesis and mechanical properties of fl ame retardant vinyl ester resin for structural composites. Polymer (Guildf) 2017;133:20–9. doi:10.1016/j.polymer.2017.11.017.
[96] Van Mele B, Rahier H, Van Assche G, Swier S. The Application of Modulated Temperature Differential Scanning Calorimetry for the Characterisation of Curing Systems 2006:83–160. doi:10.1007/1-4020-3750-3_2.
[97] Elvin N, Elvin A, Senderos BZ. Capacitance changes in thin piezoelectric transducers embedded in isotropic host materials. J Intell Mater Syst Struct 2018;29:816–29.

doi:10.1177/1045389X17721045.